Chinese Chemical Letters 37 (2026) 111557

Contents lists available at ScienceDirect

Chinese Chemical Letters

journal homepage: www.elsevier.com/locate/cclet

Fluorinate localized solvation PVDF-HFP-based polymer electrolyte producing LiF-rich interface for solid-state lithium metal batteries

Bin Wang[a], Qingqing Zhou[a], Junjie Lu[a], Chuyang Li[a], Mengmeng Fan[b,d], Wenwei Ding[a], Bifu Sheng[a], Wenjuan Zhu[a], Qian Ni[a], Huixin Chen[c,e], Xiang Han[a,*]

[a] College of Materials Science and Engineering, Co-Innovation Center of Efficient Processing and Utilization of Forest Resources, Nanjing Forestry University, Nanjing 210037, China
[b] Jiangsu Co-Innovation Center of Efficient Processing and Utilization of Forest Resources, International Innovation Center for Forest Chemicals and Materials, College of Chemical Engineering, Nanjing Forestry University, Nanjing 210037, China
[c] State Key Laboratory of Structural Chemistry, Fujian Institute of Research on the Structure of Matter, Chinese Academy of Sciences, Fuzhou 350002, China
[d] Key Lab of Biomass Energy and Material, Jiangsu Province; Jiangsu Co-Innovation Center of Efficient Processing and Utilization of Forest Resources, Institute of Chemical Industry of Forest Products, Chinese Academy of Forestry, Nanjing 210042, China
[e] Xiamen Key Laboratory of Rare Earth Photoelectric Functional Materials, Xiamen Institute of Rare Earth Materials, Haixi institutes, Chinese Academy of Sciences, Xiamen 361021, China

ARTICLE INFO

Article history:
Received 22 April 2025
Revised 2 July 2025
Accepted 8 July 2025
Available online 8 July 2025

Keywords:
Solid-state battery
PVDF-HFP based solid polymer electrolyte
Fluorinate localized solvation structure
Lithium-ion transport
Interface stability

ABSTRACT

Poly(vinylidene fluoride-*co*-hexafluoropropylene) (PVDF-HFP)-based solid polymer electrolytes show great potential for high energy lithium metal batteries, however, the residual solvent and related severe side reactions limit its development. Herein, a PVDF-HFP-based solid polymer electrolyte modified by fluorobenzene (FB) co-solvent is designed to address these problems. The introduced FB with weak solvation interaction regulates the coordination environment and induces anions to enter the solvation structure, generating more contact ion pairs (CIPs) and aggregates (AGGs). In addition, the anions-derived LiF-rich interphases help to improve the interface stability against Li metal. As a result, the FB-PVDF-HFP achieves high ionic conductivity (4.1×10^{-4} S/cm) and low activation energy (0.125 eV) at room temperature. In addition, Li||Li symmetric cells using FB-PVDF-HFP electrolyte can achieve uniform and dendrite-free lithium deposition/stripping in the long-term cycling over 2300 h. The assembled solid-state Li|FB-PVDF-HFP|LFP full cell shows improved rate performance and cycling performance (600 cycles at 0.5 C and 450 cycles at 3 C) at room temperature. This work verifies the feasibility of fluorinated terminated solid polymer electrolytes on its lithium-ion transport and interfacial stability in lithium metal batteries.

© 2026 Published by Elsevier B.V. on behalf of Chinese Chemical Society and Institute of Materia Medica, Chinese Academy of Medical Sciences.

The demand for high energy density lithium-ion batteries is rising due to the rapid growth of electric vehicles, portable electronic devices, and large-scale energy storage systems. Metallic lithium, because of its high specific capacity (3860 mAh/g), relatively low density (0.534 g/cm^3), and the lowest potential (−3.04 V), is a promising anode material for high energy density lithium metal batteries [1–8]. However, liquid organic electrolytes paired with lithium metal anode may cause severe side reactions and thick solid-electrolyte-interphases (SEI). In addition, the growth of lithium dendrites in liquid electrolyte shows safety risks such as leakage and combustion. Furthermore, the incompatibility of liquid electrolytes with high-voltage cathodes hinders further energy density advancements [9,10]. Substituting liquid organic electrolytes with solid-state electrolytes can mitigate the above-mentioned issues in lithium metal batteries. Solid-state electrolytes with high modulus is expected to suppress the formation of lithium dendrites and improve battery safety and cycle stability [11–15].

Among solid-state electrolytes, solid polymer electrolytes have attracted much attention due to their good flexibility and large scale processability [16,17]. Especially for polyvinylidene fluoride (PVDF)-based solid electrolyte, due to the strong interaction between lithium salt and residual *N*,*N*-dimethylformamide (DMF) solvent, solvated molecules can be rapidly transmitted through the polymer chain, that make it has relatively high room-temperature lithium ion conductivity (~10^{-4} S/cm) [18,19]. The ionic conductivity can be further improved by copolymerization of hexafluoropropylene with vinylidene fluoride (PVDF-HFP) [20,21]. However, there remain several problems hindering the practical application of PVDF-HFP-based solid polymer electrolytes. First, unlike

* Corresponding author.
E-mail address: hanxiang@njfu.edu.cn (X. Han).

https://doi.org/10.1016/j.cclet.2025.111557
1001-8417/© 2026 Published by Elsevier B.V. on behalf of Chinese Chemical Society and Institute of Materia Medica, Chinese Academy of Medical Sciences.

solid electrolytes such as polyethylene glycol (PEO) which form a dense membrane, the PVDF-HFP matrix consists of spherical particles with voids between them. These voids may lead to an uneven distribution of lithium ions, resulting in uncontrollable growth of Li dendrites [22]. Secondly, the interaction of lithium salt with the residual DMF solvent forms $[Li(DMF)_x]^+$ solvated molecules, which when matched with lithium metal anodes, the side reactions result in severe capacity decay of lithium metal batteries during long-term cycling [23]. Therefore, it is crucial to improve the microstructure of solid polymer electrolytes and modulate the solvation structure to ensure rapid lithium-ion transport and create a stable interfacial reaction environment [24]. Conventional strategies include organic molecule modification [25,26], inorganic filler modification [27–29], additive modification [30,31] and other [32–34], among which the use of additives is relatively common, especially fluoride additives. Because the side reaction between electrode and electrolyte may result in chemical instability and mechanical weakness of electrode-electrolyte interface, fluorine has unique chemical and physical properties-hydrophobicity, strong bonding strength and stability, excellent dielectric properties and strong electronegativity and polarization, which can well deal with these problems [35,36]. Moreover, fluorine-containing additives can also improve ion transport and define well-defined ion transport channels [37].

In this work, we designed a fluoride additive fluorobenzene (FB)-modified PVDF-HFP-based solid electrolyte (FB-PVDF-HFP), which exhibited high room-temperature ionic conductivity and excellent electrode-electrolyte interface stability. It was found that after adding FB, FB partially replaced DMF, leading to a decrease in the amount of DMF in the solvation process. This significantly reduced the side reactions between Li metal and DMF. In addition, the decomposition of FB will also generate LiF products, thus producing more LiF in the SEI layer. This ensuring the rapid transport of Li^+ in the SEI and the stability of the battery. Taking advantages of these advantages, the FB-PVDF-HFP electrolyte has an ambient ionic conductivity as high as 4.1×10^{-4} S/cm and an ion transfer number of 0.40, and the use of the FB-PVDF-HFP electrolyte enables uniform and dendrite-free Li plating/stripping during long term cycling in Li||Li symmetric cell. Solid-state Li|FB-PVDF-HFP|LFP full cells exhibit superior rate performance and cycle performance (450 cycles at 3 C).

For the preparation of composite solid electrolyte membrane, PVDF-HFP (Sigma), lithium salt (LiTFSI) (99.9 %, Canrd) and LATP (Canrd) were mixed in DMF (99.9 %, Aladdin) with a mass ratio of 10:10:1. Then, the homogenized slurry was spread on a clean glass surface and vacuum dried at 60 °C for 48 h to evaporate the residual solvent. The resulting polymer electrolyte membrane was labeled as PVDF-HFP. 2.5 % FB (99.9 %, Aladdin) additive was added in the slurry to prepare the FB-PVDF-HFP membrane.

The crystal structure of the electrolytes was characterized by X-ray diffraction (XRD) (Cu Kα, $\lambda = 0.15406$ nm). A field-emission scanning electron microscope (FESEM, JSM-7600F) was applied to monitor the surface and cross-sectional morphology of the electrolyte and Li metal after cycling. The surface chemistry of Li metal after cycling was analyzed on X-ray photoelectron spectroscope (XPS) equipment (Thermo Scientific Kα spectrometer). The TG-DSC was conducted using a German Netzsch STA 449 F3 instrument, with a heating rate of 10 °C/min from room temperature to 800 °C under an argon atmosphere. The mechanical property tests were performed using a SANS UTM2502 universal testing machine.

The electrochemical performances of the polymer electrolytes were measured by Bio-Logic VSP-300 electrochemical workstation. The ionic conductivity was determined through electrochemical impedance spectroscopy (EIS) employing stainless-steel (SS) symmetric cells. Measurements were conducted in the temperature range of 30–80 °C, with a frequency range from 7 MHz to 0.1 Hz and an AC amplitude of 20 mV. The conductivity was calculated by the following Eq. 1:

$$\sigma = L/RS \tag{1}$$

where L is the thickness of solid polymer electrolytes; R is the high-frequency intercept obtained from the electrochemical impedance spectroscopy (EIS), S is the contact area between SS and the polymer electrolyte membrane. The activation energy of the SPEs was calculated by the following Arrhenius Eq. 2:

$$\sigma = \sigma_0 \exp\left(E_a/RT\right) \tag{2}$$

where σ_0 is the per-exponential factor; E_a is the activation energy; T is the absolute temperature.

The lithium-ion migration number (t_+) was examined by combining AC impedance and DC polarization methods employing lithium symmetric cells. t_+ was calculated by the following Eq. 3:

$$t_+ = \left(I_{ss}(\Delta V - I_0 R_0)\right)/\left(I_0(\Delta V - I_{ss}R_{ss})\right) \tag{3}$$

where ΔV is the applied polarization voltage; I_0 and I_{ss} are the initial current and steady-state current, respectively; R_0 and R_{ss} are the initial resistance and steady-state resistance, respectively. The $I-t$ curve was obtained by the Bio-Logic VSP-300 electrochemical workstation and potentiostatic chronoamperometry, where ΔV was 10 mV, time t was 7200 s, the test temperature was room temperature.

To evaluate solid-state cell performance, the cathodes were prepared using a traditional slurry-coating method. $LiFeO_4$ power, carbon black, and PVDF binder (5 wt% dissolved in DMF) were mixed and dissolved in a mass ratio of 8:1:1 in *N*-methylpyrrolidone (NMP, Aladdin). The mixed slurry was spread onto the aluminum foil and dried in a vacuum drying oven at 80 °C for 12 h. The cathode was obtained with an active material mass loading of 0.9–1.4 mg/cm^2. For the CR2025 type coin cell, the cathode was cut into disks of 12 mm diameter. All the cells were assembled in an argon-filled glovebox with H_2O and O_2 < 0.1 ppm. The galvanostatic charge/discharge performances of the assembled cells were recorded between 2.8 V and 3.9 V using a Neware CT-408T-5V20mV-HWX battery test instrument.

Adsorption energy calculation is also important. All calculations were carried out by DFT as implemented in the Vienna *Ab Initio* Simulation Package (VASP) [38] with plane wave basis sets and projector-augmented wave (PAW) pseudopotentials [39]. The Perdew-Burke-Ernzerhof (PBE) generalized-gradient approximation (GGA) was adopted as the exchange-correlation function [40]. The energy cutoff of 520 eV was used for structural relaxation and energy calculations. The convergence criterion for energy and force for structural relaxation was set as 1.0×10^{-5} eV and 0.01 eV/Å, respectively. The adsorption energy E_{ads} was calculated by the following Eq. 4:

$$E_{ads} = E_{total} - E_{adsorbate} - E_{adsorbent} \tag{4}$$

where E_{total} is the total energy of the interaction system between the adsorbate and the adsorbent, $E_{adsorbate}$ is the energy of the isolated adsorbate, $E_{adsorbent}$ is the energy of the isolated adsorbent.

The FB-PVDF-HFP and PVDF-HFP electrolytes were prepared by solution casting method, then characterized and compared. The scanning electron microscope (SEM) images of PVDF-HFP and FB-PVDF-HFP electrolyte membranes are shown in Figs. 1a and b. After adding FB, the surface of the PVDF-HFP-based solid polymer electrolyte becomes denser, and the dense solid electrolyte structure can provide a shorter and more regular ion transmission channel, reduce the scattering and obstruction of ions during the transmission process, thereby improving the ion conductivity [41,42]. Moreover, FB-PVDF-HFP electrolyte has a thickness of about 80 μm (Fig. 1c) and good flexibility. As shown in Fig. S1 (Supporting information), the DSC curve exhibits no significant baseline shift or

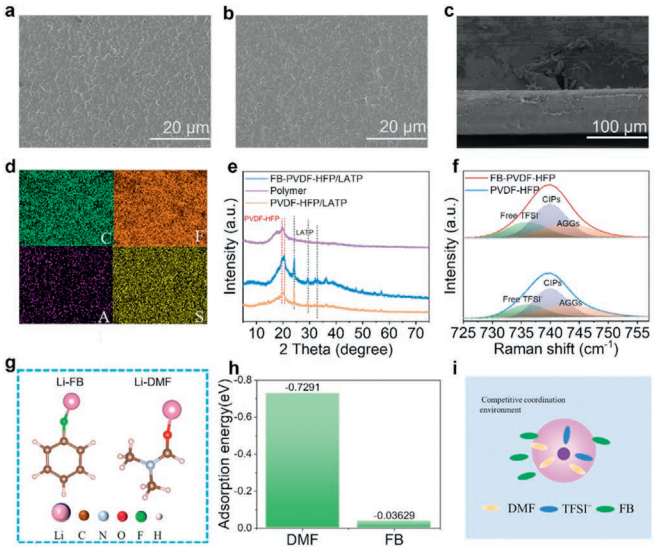


Fig. 1. Characterizations of the polymer electrolyte membranes. Surface SEM images of (a) PVDF-HFP and (b) FB-PVDF-HFP electrolytes. (c) Cross-sectional SEM image of FB-PVDF-HFP membrane. (d) EDS elemental mapping of C, F, Al, S. (e) XRD patterns of PVDF-HFP and FB-PVDF-HFP membranes. (f) The fitting results of solvation structure from Raman spectra in FB-PVDF-HFP and PVDF-HFP electrolytes (CIPs: anions coordinate with one lithium ion, AGGs: anion coordinate with two or more lithium ions). (g) The molecular structures and (h) the adsorption energy of DMF, and FB for a Li^+. (i) The solvation environment after adding FB.

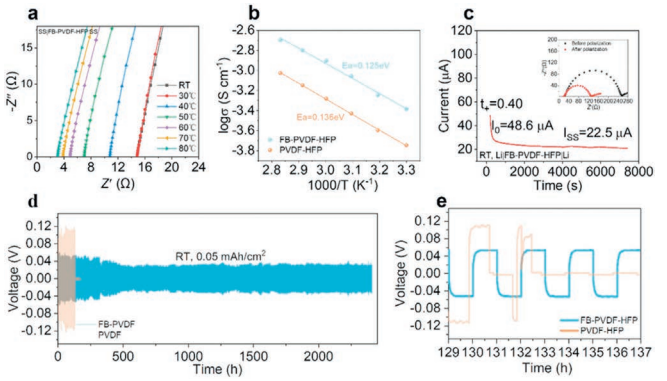


Fig. 2. Electrochemical performances of symmetric cells. (a) Nyquist plots of SS|FB-PVDF-HFP|SS cell at various temperatures. (b) Arrhenius plots of ionic conductivities for FB-PVDF-HFP and PVDF electrolytes. (c) Chronoamperometry curve of Li|FB-PVDF-HFP|Li cell under 10 mV polarization. The inset is EIS spectra before (black) and after (red). (d) Galvanostatic cycling curves of Li|FB-PVDF-HFP|Li and Li|PVDF-HFP|Li cells under 0.05 mA/cm^2 for 1 h at room temperature. (e) Enlarged plots of Fig. 2d around 130 h.

minor endothermic peaks within the temperature range from room temperature to 300 °C, which indicates that the FB-PVDF-HFP possesses a low glass transition temperature (T_g), remaining in the rubbery state above T_g at room temperature. The results prove that it has good thermal stability. FB-PVDF-HFP also has better mechanical properties (Fig. S2 in Supporting information). Fig. 1d shows the energy dispersive spectroscopy (EDS) image of the FB-PVDF-HFP electrolyte membrane, indicating that LiTFSI and LATP are uniformly dispersed in the PVDF-HFP framework, which ensures that FB-PVDF-HFP electrolyte could rapidly transport Li^+. To further confirm the crystalline nature of the polymer hosts and LATP particles, the X-ray diffraction (XRD) patterns were obtained, as shown in Fig. 1e, characteristic peaks around 19.8° and 20.1° are detected, indicating that the PVDF-HFP matrix includes α-phase PVDF-HFP, while the crystalline phase is essentially unchanged after adding FB. But we can see the peaks of PVDF-HFP width significantly broaden after the addition of FB in Fig. S3 (Supporting information), indicating a decrease in its crystallinity. The poor crystallization is expected to reduce the porosity of the PVDF-HFP film and facilitate ion transport. Raman spectroscopy was used to further reveal the coordination state of the anions. As shown in Fig. 1f, the free solvent molecules of the PVDF-HFP electrolyte and FB-PVDF-HFP electrolyte disappear, forming contact ion pairs (CIPs, anions coordinate with one lithium ion) and aggregates (AGGs, anion coordinate with two or more lithium ions), but with the addition of FB, both CIPs and AGGs begin to increase (Fig. S4 in Supporting information), indicating that FB facilitates the formation of CIPs and AGGs, which improves the ionic conductivity of the electrolyte membrane. As shown in Figs. 1g and h, the adsorption energy of Li-DMF and Li-FB were determined through theoretical calculations. Li-FB has lower adsorption energy, which proved that FB only partially replaced DMF, leading to a decrease in the amount of DMF in the solvation process (Fig. 1i).

Ionic conductivity is a key parameter for the electrochemical performance of solid electrolytes. Symmetrical cells using stainless-steel (SS) as blocking electrodes were assembled to measure the ionic conductivity of the solid polymer electrolyte. According to the electrochemical impedance spectra (EIS), the ionic conductivity of the FB-PVDF-HFP electrolyte can be calculated to be 4.1×10^{-4} S/cm at room temperature, which is much higher than that of the PVDF electrolyte (1.97×10^{-4} S/cm, Fig. S5 in Supporting information). It is because of the introduction of FB, which induces anions into the solvated structure, and the anions cooperate with FB to weaken the interaction between PVDF and DMF solvent, thus ensuring rapid transport of Li^+ [43]. Fig. 2a and Fig. S6 (Supporting information) show the variable temperature ionic conductivity of solid polymer electrolytes at 30–80 °C. As the temperature increases, the ionic conductivity gradually increases. This is because the chain segments and volume of the polymer matrix PVDF-HFP are affected by temperature. The increase in temperature causes the free volume to expand and accelerates the movement of the polymer chain segments, resulting in an incensement in ionic conductivity [44]. The Arrhenius plot (Fig. 2b) based on the ionic conductivity at different temperatures shows that the activation energy of FB-PVDF-HFP and PVDF-HFP electrolytes are 0.125 and 0.136 eV, respectively, which indicates that the Li-ion migration barrier is lower in FB-PVDF-HFP polymer electrolyte. Lithium-ion transfer number (t_+) is another important indicator for evaluating the Li-ion migration capability of electrolytes, the t_+ of FB-PVDF-HFP is 0.40 (Fig. 2c), which is higher than that of PVDF electrolyte ($t_+ = 0.28$, Fig. S7 in Supporting information), which is profited from the accelerated interfacial Li-ion transport in FB-PVDF-HFP. The electrochemical performances of the polymer solid-state electrolyte with and without FB in contact with lithium metal anodes were further tested by assembling the Li||Li symmetrical battery to investigate the effect of FB on the stability of the Li/electrolyte interface. As shown in Figs. 2d and e, the Li|FB-PVDF-HFP|Li symmetric cell exhibits stable cycling performance for over 2000 h at a current density of 0.05 mA/cm^2 at room temperature, whereas the Li|PVDF-HFP|Li cell short circuits after only 130 h. Meanwhile, the low Li-ion conductivity as well as the thick SEI of the PVDF-HFP electrolyte leads to an ultra-high overpotential, which hinders the efficient electrochemical cycling of the Li|PVDF-HFP|Li symmetric cell. It is because the side reactions between Li metal and free DMF molecules, causing the overpotential of the Li|PVDF-HFP|Li symmetric cell to continuously increase, leading to short circuiting after approximately 130 h of cycling. The introduction of FB modulates the solvation structure (more CIPs and AGGs), FB partially replaces DMF, leading to a decrease in the amount of DMF in the solvation process. This significantly reduces the side reactions between Li metal and DMF. In addition, the decomposition of FB

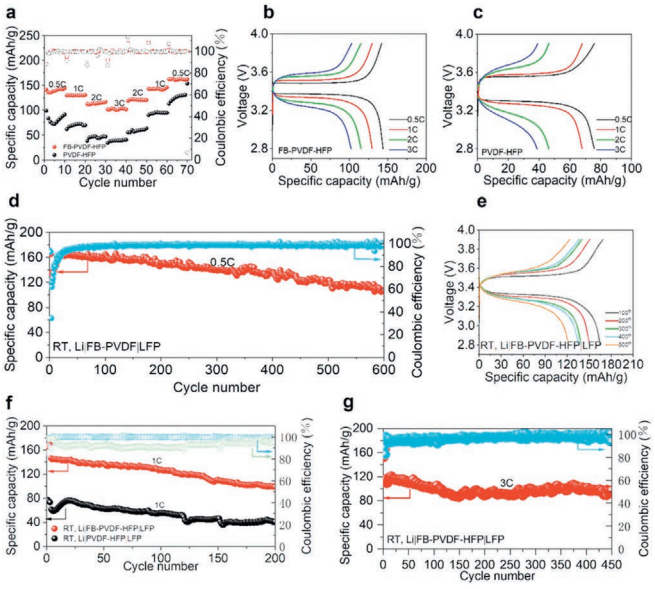


Fig. 3. Cycling and rate performance of full cells at room temperature. (a) Rate capability of Li|FB-PVDF-HFP|LFP and Li|PVDF-HFP|LFP cells. Charge/discharge curves of (b) Li|FB-PVDF-HFP|LFP and (c) Li|PVDF-HFP|LFP under different rates. (d) Cycling performance of Li|FB-PVDF-HFP|LFP cell at 0.5 C. (e) Charge/discharge curves of Li|FB-PVDF-HFP|LFP under different cycle. (f) Cycling performance of Li|FB-PVDF-HFP|LFP and Li|PVDF-HFP|LFP cells at 1.0 C. (g) Cycling performance of Li|FB-PVDF-HFP|LFP at 3.0 C.

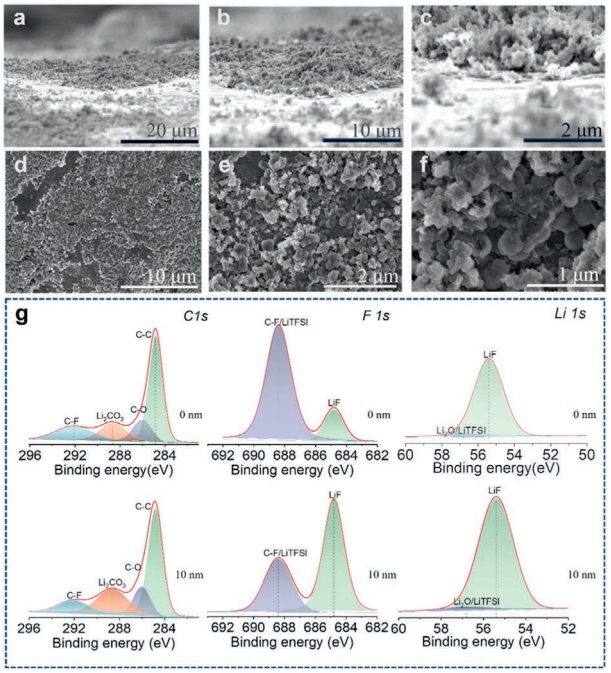


Fig. 4. Characterization of Li metal after cycling. (a-c) Cross-sectional SEM of the cycled Li metal using FB-PVDF-HFP at different scales. (d-f) Surface SEM of the cycled Li metal using FB-PVDF-HFP at different scales. (g) XPS spectra of SEI on Li metal in Li|FB-PVDF-HFP|Li cell.

will also generate LiF products, thus producing more LiF in the SEI layer, thus ensuring long-term stable cycling.

To further evaluate the electrochemical performance of FB-PVDF-HFP electrolyte, Li|FB-PVDF-HFP|LFP and Li|PVDF-HF-P|LFP full cells were assembled and measured at room temperature in the voltage range of 2.8–3.9 V. As shown in Fig. 3a, the capacities of Li|FB-PVDF-HFP|LFP cells are 142.1, 129.8, 115.2 and 102.3 mAh/g at 0.5, 1, 2 and 3 C, respectively, and the capacity remains basically unchanged when the current density returns to 0.5, 1, 2 and 3 C, the excellent rate capability benefits from the fast Li-ion transfer kinetics in the FB-PVDF-HFP electrolyte. The charge-discharge profiles of the Li|FB-PVDF-HFP|LFP battery at different rates are stable, indicating that no side reactions occur (Fig. 3b). On the contrary, Li|PVDF-HFP|LFP cell showed lower capacity at the same rate (Fig. 3c). The Li|FB-PVDF-HFP|LFP cell demonstrates excellent cycling stability, maintaining high capacity and coulombic efficiency over extended periods. Specifically, it can cycle for over 500 cycles at 0.5 C, retaining a capacity exceeding 120 mAh/g and achieving a coulombic efficiency close to 99.9 % (Figs. 3d and e). Moreover, it exhibits stable cycling for 200 cycles at 1 C with the capacity of approximately 100 mAh/g, outperforming the Li|PVDF-HFP|LFP counterpart which only reaches about 40 mAh/g after 200 cycles at 1 C (Fig. 3f). Additionally, the Li|FB-PVDF-HFP|LFP cell can also maintain stability cycle up to 450 cycles at 3 C (Fig. 3g).

To further investigate the effect of FB-PVDF-HFP on lithium deposition, the recycled cells were disassembled in the argon glove box, and the recycled lithium sheets were characterized to investigate the interface of the cells. As shown in Figs. 4a-c, the SEM images of the cross-section of the lithium metal after cycling, reveal messy lithium dendrites produced on the surface. which further proves that LiF-rich inorganic materials are formed on the surface of the cathode throughout the cycling process. Dense spherical lithium can be observed on lithium sheet when using FB-PVDF-HFP electrolyte (Figs. 4d-f), which can effectively minimize the side reaction between the lithium anode and the electrolyte and inhibit the growth of lithium dendrites after the formation of this compact lithium deposition, while the PVDF-HFP electrolyte is more likely to form lithium dendrites (Fig. S8 in Supporting information), indicating that the incorporation of FB hinders the growth of lithium dendrites to some degree. The compositions of SEI from the cycled Li metal anode surface were further analyzed by

X-ray photoelectron spectroscopy (XPS). As shown in the C 1s spectra, four distinct peaks at 285.2, 286.5, 288.6 and 292.1 eV were fitted and assigned to C–C, C–O, Li_2CO_3 and C-F, respectively. Furthermore, as shown in the F 1s spectra, two distinct peaks at 684.8 and 688.1 eV were fitted and assigned to LiF and C-F/LiTFSI, respectively. Meanwhile, two distinct peaks at 56.8 and 55.4 eV were fitted and assigned to Li_2O/LiTFSI and LiF, respectively, as shown in Li 1s spectra. The XPS (Fig. 4g) further illustrates that the cathode surface formed an inorganic interface layer rich in LiF. As an excellent electronic insulator, LiF can prevent the transmission of electrons, inhibit the side reaction between lithium metal and the electrolyte effectively. Compared with the traditional SEI, LiF has better ionic conductivity and chemical stability, but also can promote the uniform deposition of lithium [45].

In summary, a PVDF-based solid electrolyte for room temperature lithium metal batteries with fast ion transport capability and long-term stable cycling was successfully prepared by adding FB. After adding FB, FB partially replaces DMF, leading to a decrease in the amount of DMF in the solvation process. This significantly reduces the side reactions between Li metal and DMF. In addition, the decomposition of FB will also generate LiF products, thus producing more LiF in the SEI layer, thereby improving the ionic conductivity and interface stability of the polymer electrolyte, allowing solid-state lithium metal cells to cycle stably for a long time. This work verifies the feasibility of fluorinated solvents in improving the ionic conductivity and interfacial stability of solid polymer electrolytes, and provides ideas for promoting the development of SSLBs based on solid polymer electrolytes.

CRediT authorship contribution statement

Bin Wang: Writing – original draft, Methodology, Formal analysis. **Qingqing Zhou:** Validation, Data curation. **Junjie Lu:** For-

mal analysis, Data curation. **Chuyang Li:** Validation, Software. **Mengmeng Fan:** Project administration, Methodology. **Wenwei Ding:** Visualization. **Bifu Sheng:** Methodology. **Wenjuan Zhu:** Methodology. **Qian Ni:** Software, Methodology. **Huixin Chen:** Resources, Data curation. **Xiang Han:** Writing – review & editing, Supervision, Conceptualization.

Declaration of competing interest

The authors declare that they have no known competing financial interests or personal relationships that could have appeared to influence the work reported in this paper.

Acknowledgments

This work was financially supported by Nanjing Forestry University and China State Shipbuilding Corporation limited (No. J063-WB-2024–2586-Y). We also thank Postgraduate Research & Practice Innovation Program of Jiangsu Province (No. KYCX25_1406).

Supplementary materials

Supplementary material associated with this article can be found, in the online version, at doi:10.1016/j.cclet.2025.111557.

References

[1] H. Wan, J. Xu, C. Wang, Nat. Rev. Chem. 8 (2024) 30–44.
[2] S.C. Kim, J. Wang, R. Xu, et al., Nat. Energy 8 (2023) 814–826.
[3] X.Y. Yu, Y.X. Huang, Y.G. Zhang, et al., Nat. Commun. 14 (2023) 2883.
[4] L. Wang, S. Xu, Z. Wang, et al., eScience 3 (2023) 100090.
[5] T. Yi, E. Zhao, Y. He, et al., eScience 4 (2024) 100182.
[6] X. Li, L. Zhang, Y. Fan, et al., Chin. Chem. Lett. 36 (2025) 109776.
[7] S. Zhao, J.J. Lu, B.F. Sheng, et al., Chin. Chem. Lett. 36 (2025) 110008.
[8] H.X. Chen, C. Zhao, H. Yue, et al., Chin. Chem. Lett. 36 (2025) 109650.
[9] B. Song, L. Su, X. Liu, et al., Electron 1 (2023) e13.
[10] J.J. Lu, B.F. Sheng, M.F. Chen, et al., Energy Storage Lett. 71 (2024) 103570.
[11] D. Zhang, Y. Liu, D. Li, et al., Energy Environ. Sci. 18 (2025) 227–235.
[12] E. Gabriel, C. Ma, K. Graff, et al., eScience 3 (2023) 100139.
[13] R.X. Wang, W.L. Feng, X. Yu, et al., eScience 4 (2024) 100274.
[14] Y. Hou, Z. Huang, Z. Chen, et al., Nano Energy 97 (2022) 107204.
[15] P. Lennartz, B.A. Paren, A. Herzog-Arbeitman, et al., Joule 7 (2023) 1471–1495.
[16] Z.C. Huang, T. Huang, X. Ye, et al., Appl. Surf. Sci. 605 (2022) 154586.
[17] P.B. Zhai, Z.L. Yang, Y. Wei, et al., Adv. Energy Mater. 12 (2022) 2200967.
[18] X. Zhang, S. Wang, C.J. Xue, et al., Adv. Mater. 31 (2019) 1806082.
[19] D. Xu, J.M. Su, J. Jun, et al., Adv. Energy Mater. 9 (2019) 1900611.
[20] W.Y. Liu, C.J. Yi, L.P. Li, et al., Angew. Chem. 133 (2021) 13041–13050.
[21] X. Zhang, J. Han, X.F. Niu, et al., Batteries Supercaps 3 (2020) 876–883.
[22] Y.X. Wang, H.J. Wang, K. Liu, et al., RSC Adv. 11 (2021) 30734–30743.
[23] K. Yang, J.B. Ma, Y.H. Li, et al., J. Am. Chem. Soc. 146 (2024) 11371–11381.
[24] W.J. Yang, Y.W. Liu, X.Y. Sun, et al., Angew. Chem. 136 (2024) e202401428.
[25] S. Zhang, Y. Lu, K. He, et al., New J. Chem. 46 (2022) 21640–21647.
[26] Y.F. Huang, T. Gu, G. Rui, et al., Energy Environ. Sci. 14 (2021) 6021–6029.
[27] W. Huang, S. Wang, X. Zhang, et al., Adv. Mater. 35 (2023) 2310147.
[28] Y. Yuan, L. Chen, Y. Li, et al., Energy Mater. Devices. 1 (2023) 9370004.
[29] P. Shi, J. Ma, M. Liu, et al., Nat. Nanotechnol. 18 (2023) 602–610.
[30] S. Zhou, S. Zhong, Y. Dong, et al., Adv. Funct. Mater. 33 (2023) 2214432.
[31] P. Yao, B. Zhu, H. Zhai, et al., Nano Lett. 18 (2018) 6113–6120.
[32] R. Razaq, M.M.U. Din, D.R. Småbråten, et al., Adv. Energy. Mater. 14 (2024) 2302897.
[33] Y.H. Wu, Y.Y. Zhao, Q.X. Yuan, et al., Nat. Commun. 15 (2024) 10843.
[34] J.W. He, Y.Y. Zhao, Y. Li, et al., Nano-Micro Lett. 17 (2025) 1–16.
[35] T. Shiga, Y. Kato, H. Kondo, et al., J. Mater. 5 (2017) 5156–5162.
[36] N. Von Aspern, G.V. Röschenthaler, M. Winter, et al., Angew. Chem. Int. Ed. 58 (2019) 15978–16000.
[37] Y.Q. Wang, Z.Z. Wu, F.M. Azad, et al., Nat. Rev. Mater. 9 (2024) 119–133.
[38] G. Kresse, J. Furthmüller, Comput. Mater. Sci. 6 (1996) 15–50.
[39] G. Kresse, D. Joubert, Phys. Rev. B 59 (1999) 1758–1775.
[40] K. Burke, J.P. Perdew, D.C. Langreth, Phys. Rev. Lett. 73 (1994) 1283–1286.
[41] D.J. Chen, Y.P. Liu, C. Feng, et al., Electron 1 (2023) e1.
[42] D.B. Li, H. Liu, C. Wang, et al., Adv. Funct. Mater. 34 (2024) 2315555.
[43] Q.J. Liu, Z.Q. Zeng, M.S. Qin, et al., Batteries Supercaps 7 (2024) e202400034.
[44] J. Jie, Y.L. Liu, L.N. Cong, et al., J. Energy Chem. 49 (2020) 80–88.
[45] O.W. Sheng, J.H. Zheng, Z.J. Ju, et al., Adv. Mater. 32 (2020) 2000223.